JOURNAL OF PROPULSION AND POWER
Vol. 15, No. 4, July–August 1999

Analyses and Application of Gas Sampling to Scramjet Engine Testing

Tohru Mitani,* Masahiro Takahashi,† Sadatake Tomioka,† Tetsuo Hiraiwa,† and Kouichiro Tani†
National Aerospace Laboratory, Miyagi 981-15, Japan

Gas sampling has been used in combustor studies and in scramjet engine testing. Because the gas sampling is based on the assumption that the gas composition is frozen in the sampling process, the critical Damkohler numbers necessary to quench reactions in the gas-sampling probes were evaluated using a reduced kinetic model. The phase plane analysis showed that reactions in probes can be extinguished if the probe Damkohler number is less than about 10. The analytical results were confirmed by numerical calculations using full kinetics. The shock swallowing into sampling probes was examined using numerical simulations for the low-Reynolds-number flow. These theoretical results were verified by experiments using four kinds of probes with various configurations in a Mach 2.5 supersonic combustor. Based on the results, fine sampling probes with a tip diameter less than 0.3 mm are recommended for scramjet testing. Based on these calibration studies, gas sampling was successfully applied to scramjet engine testing under a flight Mach number up to 8, to reveal interesting features in the internal flow in swept-back engines.

Nomenclature

$C_{m,i}$ = influential coefficient of local mass flux to variable, i
c_p = specific heat of sampled gas
Da = Damkohler number, x_c^*/x_r^*
d = diameter of tip orifice
E_1 = activation energy of reaction 1
k_i = rate constant of reaction i
k_q = rate constant or radical quenching reactions
M = Mach number
m = mass flux through sampling orifice or in engine
Nu = Nusselt number for tip flow
P_s = static pressure
P^0 = total pressure
Ta = air total temperature supplied by the $M2.5$ vitiation air heater
T_s = static temperature in probe flow
Tw = tube wall temperature of probes
T^0 = total temperature
t_r = reaction time of R_1, $1/k_1(O_2)$
U = flow velocity
X = nondimensional radical mole fraction
x = streamwise distance along probes
x_c^* = characteristic cooling length, Eq. (2)
x_r^* = characteristic reaction length, $U \times t_r$
α = nondimensional heat of breaking reaction
β = nondimensional breaking reaction rate
ΔP^0 = loss of P^0 in pitot measurement
η_c = local combustion efficiency
θ = nondimensional temperature, T/T_0
θ_w = nondimensional temperature, Tw/T_0
κ = thermal diffusivity of gas
λ = thermal conductivity of gas
ξ = streamwise distance nondimensionalized by x_c^*
Φ = total fuel equivalence ratio in engine
χ = local equivalence ratio of H_2

Subscript

0 = initial value

Introduction

IN the National Aerospace Laboratory, H_2-fueled scramjet engines have been tested. The scramjet engine can deliver thrust increments of 1300 N ($M4$) and 1100 N ($M6$) with H_2 combustion. The thrust/drag performance, the evolution of combustion in the engine, and the dependency of engine performance on test air are summarized in Refs. 1–3. We use three independent measurements of engine thrust: the scale-force method using the force balance, the internal force estimation by integration of wall pressure, and the momentum balance method measured at the exit of the engine. The combustion efficiency, the fluxes of mass, impulse function, and enthalpy were measured by using gas sampling. The performances determined by the three methods were compared to improve the confidence in the thrust data.

Gas sampling is based on the assumption that the gas composition is frozen in the sampling process. Preservation of major species, however, becomes difficult under scramjet testing conditions. Billig et al.[4] proposed a steam calorimeter to measure the bulk combustion efficiency, in which water was sprayed into the hot exhaust stream to quench the reaction. However, according to the ignition time of the H_2/air mixture and the flow velocity in the scramjet, the distance permitted for cooling is less than 10 mm. This cooling rate is difficult to achieve in the spray device, as discussed by Mitani et al.[5] The cooling rate may be attained in microprobes because the heat transfer rate can be accelerated adjusting the fine orifices. The probing is a pointwise measurement, and the measurements should be repeated to evaluate the overall properties of flow. However, this troublesome work gives very useful information to understand the mixing and combustion process taking place in the scramjet engines, because air and fuel are not evenly distributed and reaction rates are restricted in the supersonic flow. Thus, we conclude that the sampling probes are more promising and informative in scramjet engines.

In gas-sampling experiments conducted by Anderson and Gooderum,[6] however, no significant amounts of unreacted H_2 and O_2 were found together in any single sample. In Refs. 6–8 it was concluded that it was impossible to quench reactions in gas-sampling probes under scramjet conditions. On the other hand, Masuya et al.[9,10] and Chinzei et al.[11] conducted supersonic-combustor experiments utilizing similar probes, and found coexisting H_2 and O_2. These contradictory results on gas sampling should be investigated to facilitate the application of gas sampling to scramjet testing.

Received 7 March 1998; presented as Paper 98-1590 at the AIAA 8th International Space Planes and Hypersonic Systems and Technologies Conference, Norfolk, VA, 27–30 April 1998; revision received 2 October 1998; accepted for publication 23 October 1998.

*Chief of Ramjet Combustion Section, Kakuda Research Center, Ramjet Propulsion Division, Kimigaya, Kukuda.

†Researcher, Kakuda Research Center, Ramjet Propulsion Division, Kimigaya, Kukuda.

The objectives of this paper are threefold. First, we treat the flow inside the probes as a reactive, and the Rayleigh flow to derive the critical Damkohler number for quenching. The critical Damkohler number is derived analytically in the phase plane on temperature and radical concentration. We also utilize a Navier–Stokes code to investigate the friction–choking in sampling probes. Second, to verify these theoretical results, we investigate gas compositions and pitot pressure using probes with various configurations in a Mach 2.5 supersonic combustor. Finally, we present our results obtained by gas sampling in scramjet engine testing and note how informative the probing is.

Reactive Flow in Probes and Phase Plane

The one-dimensional reactive flow in the gas-sampling tube was analyzed by Mitani.[12] When nondimensional temperatures of the sampled gas and the tube wall are denoted as θ and θ_w, respectively, the nondimensional form for T^0 is written as

$$\frac{\mathrm{d}\theta}{\mathrm{d}\xi} = -(\theta - \theta_w) \tag{1}$$

where the streamwise distance is nondimensionalized using the cooling length (x_c^*), expressed by Nusselt number as follows:

$$x_c^* = \frac{c_p m}{\pi Nu \lambda} \tag{2}$$

A simplified reaction model is considered, which consists of a branching reaction with a strong temperature dependence and a breaking reaction. In the model, a radical is formed by the branching reaction, $H + O_2 \rightarrow O + OH$ (reaction: R_1) in H_2/air systems, and transformed to a product by breaking reactions, $OH + H + M \rightarrow H_2O + M$ or $H + O_2 + M \rightarrow HO_2 + M$. Thus, the concentrations of radicals (X) is determined by

$$\frac{\mathrm{d}[X]}{\mathrm{d}x} = \frac{1}{U}\left\{k_1[O_2][X] - k_q[M][X]^2\right\}$$

$$= \frac{1}{x_r^*}\left\{X \exp\left(-\frac{E_1}{R^0 T_s}\right) - \beta X^2\right\} \tag{3}$$

where the nondimensional radical concentration (X) is defined employing the initial value, and the breaking reaction rate is denoted by

$$\beta = \frac{k_q[M][X]_0}{k_1[O_2]} \tag{4}$$

Catalytic reactions on the tube wall have been neglected in Eq. (3), because the surface reactions break radicals to promote the quenching of sampled gas without heat addition. The reaction length (x_r^*) is given as a product of the reaction time (t_r) and the flow speed (U). When we nondimensionalize Eq. (3) with x_c^* we obtain the following equations:

$$\frac{\mathrm{d}X}{\mathrm{d}\xi} = Da\left[X \exp\left\{\theta_a\left(1 - \frac{1}{\theta}\right)\right\} - \beta X^2\right] \tag{5}$$

$$Da = \frac{c_p m}{\pi Nu 1}\frac{B_1[O_2]\exp(-\theta_a)}{U} \propto \frac{Pd^2}{4kNu}\exp\left(\frac{-8450}{T_{s0}}\right) \propto Pd^2 \tag{6}$$

in which B_1 expresses the pre-exponential factor, and θ_a denotes the Zel'dovich number ($\equiv E_1/R^0T_0$) for the R_1. Equation (6) yields $Da \propto (P \times d)^2$, if we use an approximation, $\kappa \propto 1/P$, which indicates how important the tip orifice diameter is.

The exothermicity of radical breaking reactions is often neglected, as in Ref. 12. However, we have considered the radical breaking reactions in the governing equation for radicals in Eq. (5) to take account of the quenching of reactions. We, therefore, add the heating effect of radical breaking to the energy equation given by Eq. (1) to obtain

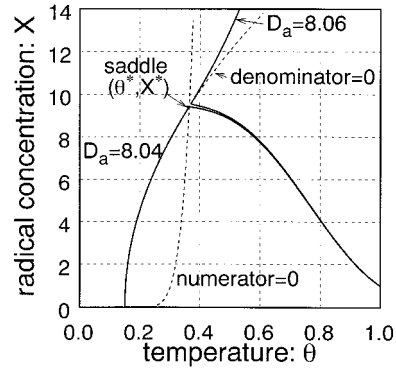

Fig. 1 Solutions for reaction quenching and thermal runaway in phase plane ($\theta_w = 0.15, b = 10^{-4}$).

$$\frac{\mathrm{d}\theta}{\mathrm{d}\xi} = -(\theta - \theta_w) + Da\alpha\beta X^2 \tag{7}$$

where the new parameter α expresses the heat of reaction in radical breaking reactions relative to the enthalpy of sampled gas.

Because the newly introduced heating term competes with the heat-loss term in Eq. (7), the solutions change drastically. To investigate the behavior of the solution, let us eliminate the independent variable ξ to construct the phase plane shown in Fig. 1 for the temperature and the radical concentration:

$$\frac{\mathrm{d}X}{\mathrm{d}\theta} = \frac{Da\left[X \exp\left\{\theta_a\left(1 - \frac{1}{\theta}\right)\right\} - \beta X^2\right]}{-(\theta - \theta_w) + Da\alpha\beta X^2} \tag{8}$$

Because of the competing terms, the denominator may vanish to form a singular point (θ^*, X^*) on the phase plane. The location of the singular point is given by the point at which the two lines, defined by the denominator $= 0$ and the numerator $= 0$, intersect. The linearization around it indicates that the singularity is a saddle point.

Examples of solutions on the phase plane are found in Fig. 1, where trajectories with two values of $Da = 8.04$ and 8.06 are illustrated. The broken line rising from $\theta = 0.3$ and approaching $\theta = 0.4$ denotes the line given by the numerator $= 0$. The other broken line raising from $\theta = 0.15$ is given by the denominator $= 0$. The quenching solutions must leave the initial condition (1, 1) with gradients, Da, to approach (θ^*, X^*), and finally, fall to the stable node (θ_w, 0) along the broken line defined by the denominator $= 0$. For a small Da, solutions run across the line by the numerator $= 0$ to reach the quenching at (θ_w, 0). However, when Da is large, solutions pass the line by the denominator $= 0$ vertically, and blow up to another limit (∞, ∞). This limit is the thermal runaway, where the deficient reactants are consumed completely.

The phase plane shows that $Da = 8.04$ leads to the quenching solution, and $Da = 8.06$ yields the thermal runaway for the combination of parameters in Fig. 1. Thus, the critical Da is determined to be 8.05. The critical Da corresponds to the condition defining the separatrix running from the initial point (1, 1) to the saddle (θ^*, X^*). The critical Da for reaction quenching increases with decreasing β or θ_w, which implies that reactions are more easily quenched in such conditions. However, the dependencies are found to be weak. Thus, the critical Da is evaluated to be about 10.

Simulations Using Numerical Codes

We constructed a one-dimensional reaction code with full kinetics, including convective heat transfer (similar to the Lewis General Chemical Kinetics and Sensitivity Analysis code now available from NASA[13]). We initiated the calculations by specifying the Mach number, static pressure, temperature, gas compositions, and Nusselt

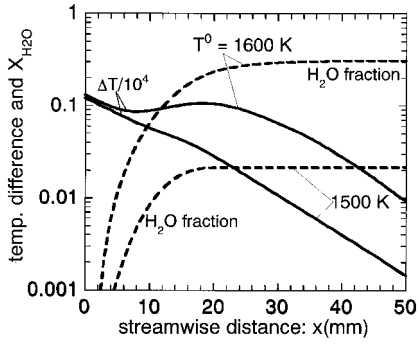

Fig. 2 Numerical simulation of thermal runaway in sampling probes by a full-kinetic code.

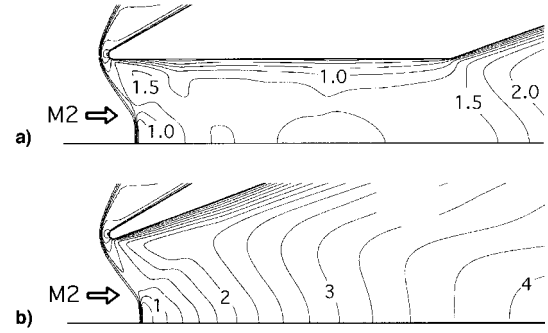

Fig. 3 Mach number contours calculated by a viscous code (a free-stream Mach number = 2).

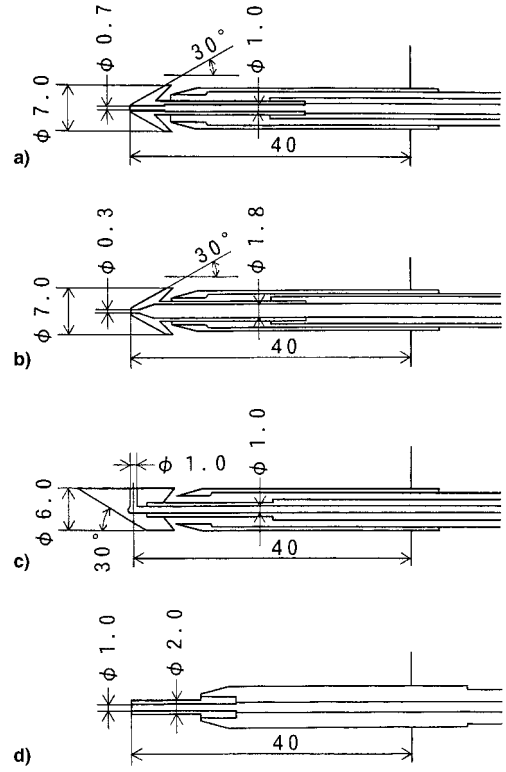

Fig. 4 Freezing- and reaction-oriented probes used for reaction quenching experiments.

number in probes. Figure 2 illustrates typical variations of the temperature difference between the gas and tube wall, $T - T_w$ (the solid lines), and the H_2O fraction formed in the probes (the broken lines). The calculation was conducted for a straight tube with a diameter of 1 mm, a static pressure of 0.1 MPa, and a sampling rate of 60 cc/s. If there is no heat release in the probe, the temperature difference should vary linearly with distance in the semilog plot. In fact, the temperature difference decreases linearly for the case of $T_0^0 = 1500$ K. Only a small heat release is observed around $x = 15$ mm, where H_2O of 2.1% is formed. In this case, the reaction is quenched there and no more H_2O is produced.

In the case of $T_0^0 = 1600$ K, heat release is initiated from $x = 6$ mm, and the concentration of H_2O increases rapidly. Consequently, the gas temperature begins to increase from $x = 7.5$ mm. The raised temperature accelerates reactions to the equilibrium state, in which the reactants are completely converted to the product, H_2O. Finally, the gas containing 31% H_2O is cooled along the probe. This is the thermal runaway found in the phase plane analysis.

Figure 2 shows that the quenching criterion is satisfied for the gas with $T_0^0 = 1500$ K, but not in the case of $T_0^0 = 1600$ K in the sampling condition. These calculations are performed assuming that the flow is decelerated to subsonic in the probe with a tip diameter of 1 mm. This calculated condition is a more hostile condition to freeze reactions than that in usual sampling, where a smaller sampling rate of less than 10 cc/s is chosen to reduce the heat capacity of gas and a finer sampling orifice (d) is employed to intent supersonic suction of gas. The supersonic operation in the tip internal flow (shock swallowing) is desirable, and reducing the tip diameter is effective for quenching reactions in gas sampled at higher temperatures.

Reducing the tip size decreases the Reynolds number, and viscous effects become dominant. It promotes friction choking in the tip and causes a strong shock wave ahead of the tip. Heating of sampled gas by the shock wave may trigger reactions in probes. We therefore simulated the viscous flow with $Re \approx 1 \times 10^2$ with a viscous (nonreactive) code to investigate the flow structure around probes inserted in Mach 2 flow (Fig. 3). The calculation was conducted for probes with a tip diameter of 0.3 mm, shown in Fig. 4b. Mach number contour maps are shown in Fig. 3. Figure 3a indicates the formation of a λ-shaped shock wave inside the tip. The Mach reflection is not a result of the straight section, because a similar shock pattern is found in Fig. 3b, where no straight section exists. The Mach reflection is caused by the detached bow shock formed at the tip edge with a finite curvature. The sampled gas, therefore, is heated by the normal shock in the central part of any sampling probe.

In Fig. 3a, the Mach number contour shows the development of the boundary layer inside the straight section. The flow, which accelerates and decelerates around $M \approx 1$ in the straight section, is the friction choking. On the other hand, Fig. 3b shows the expanded flow accelerated to supersonic speed just behind the normal shock. This acceleration is favorable for quenching the reaction, because the static temperature and pressure decrease. Thus, shortening of the straight section is effective for intermitting the reactions in sampled gas.

Strong pressure gradients between the shock and the probe tip may cause preferential deflection of light-gas species around the probes, so that the sample may be enriched with heavy-gas species (preferential sampling effect).[14,15] However, Fig. 3 shows that the preferential sampling effect does not occur in these probes because the normal shock is formed inside the orifice and the standoff distance from the leading edges of tips is negligible compared with the tip diameter. To confirm this, we examined the mass conservation of H_2 and air at the entrance and exit of the combustion duct. There were no H_2 defects in the gas compositions sampled at the exit of the engine nor in the direct-connect supersonic combustor. We therefore concluded that the preferential sampling effect was not significant.

Experimental Validations

To assess the reaction quenching in probes, we used a supersonic combustor (vitiation air heater), operating with an airflow of M2.5 and a Ta up to 2250 K. The combustor was used as a supersonic flow reactor to calibrate the sampling technique. Variations in gas composition and pitot pressure were measured at the exit of the combustion duct (dimensions = $94.3W \times 87H$). Details of experiments are found in Ref. 5.

We designed four kinds of gas-sampling probes: freezing-oriented, reaction-oriented, and static pressure-type probes shown in Fig. 4. The water-cooled, freezing-oriented probe (Figs. 4a and 4b) has a 30-deg half-angle conical tip with a passage on the centerline

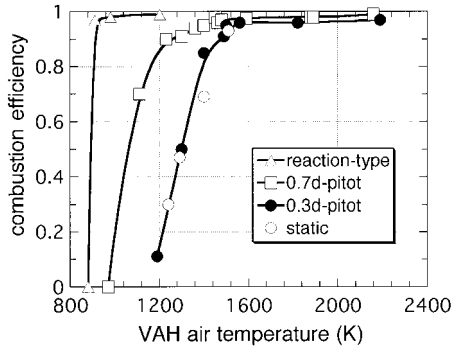

Fig. 5 Combustion efficiency of H_2 measured by various probes in the $M2.5$ combustor.[5]

for pitot pressure measurement and gas-sampling withdrawal. The baseline probe (Fig. 4a) has a tip diameter of 0.7 mm with a 6-mm straight section following it. Probe Fig. 4b has a minimum passage diameter of 0.3 mm and a 0.6-mm straight section. The static-type probe (Fig. 4c) has a tip diameter of 1 mm to grasp the external flow across the boundary layer on the probe surface. The effectiveness of the freezing-oriented probes can be examined by comparison with the reaction-oriented probes (Fig. 4d). This probe is a pitot type to promote reactions ahead of and inside it. The probe is made of nickel to promote the catalytic effect, and it is not water cooled.

A 10-probe (probe pitch = 10 mm) rake was used to measure local, spanwise distributions of gas compositions and pitot pressure at the centerline of the duct exit. The gas-sampling experiments were repeated, replacing the four different probe rakes. Wall pressure was measured at 50 stations along the supersonic combustor in this probe-calibration study. The probes shown by Fig. 4c often indicated erroneous static pressure. Because the flow direction is initially unknown, in-stream data of static pressure were not used in this experiment. Ignition triggered by probes was examined by observing flames with/without probing rakes. There was no triggered ignition except for the reaction-oriented probe (Fig. 4d).

Figure 5 summarizes the dependence of η_c measured at the central core region on the total temperature of air, Ta. Static temperature is more relevant to discuss ignition and combustion. However, the static temperature is not the controllable parameter in this experiment, because heat release changes the flow Mach number, and then the static temperature. Therefore, the controllable variable Ta was chosen in the figure. The static temperature corresponding to the critical ignition of $Ta = 1200$ K, as discussed later, is ~550 K, which is much lower than the usual ignition limit temperature of H_2 (~1000 K). It implies that the ignition in the core flow may be induced by a recompression shockwave at the duct exit, and assisted by radicals supplied from the combustion heater.[2]

The reaction-oriented probes showed a clear-cut behavior of $\eta_c = 0$ or 1.0 between $Ta = 875$ and 910 K. That is, all of the H_2 remains unburned for $Ta < 875$ K, and the H_2 is consumed completely if $Ta > 910$ K. This is clearly the autoignition of the H_2–air premixture triggered with the reaction-oriented probes. Thus, the reaction-oriented probes indicates a high, but false combustion efficiency in supersonic combustor experiments.

Because heating across the shock wave is absent in the static pressure-type probes shown by Fig. 4c, the results obtained by the static probes represent the standard of frozen gas compositions. Figure 5 shows that the data by the $0.3d$ probes agree with those by the static probes. The static-type and the $0.3d$ probes indicate that the combustion is initiated when the Ta exceeds 1200 K. A faint luminous flame, which was observed for $Ta > 1200$ K, indicates this. These experimental facts indicate that the combustion actually began at $Ta = 1200$ K, and that the $0.3d$ probes correctly detected and measured the combustion in the combustor. However, the $0.7d$ probes mislead the occurrence of combustion at $Ta = 1100$ K and a higher η_c of about 90% at $Ta = 1200$ K in Fig. 5. Thus, quenching of reactions in the $0.7d$ probes is insufficient. This is the reason why inconsistent results have been reported in Refs. 6–11.

The third piece of evidence showing combustion at $Ta > 1200$ K was obtained from pitot pressure measurements. The initiation of combustion could be detected by drops in pitot pressure. The pitot pressure measured at the core region and the wall pressure at the duct exit are illustrated with changing Ta in Fig. 6. Both the pressures are normalized by the total pressure of the vitiation air heater. The pitot pressure for $Ta < 1200$ K do not depend on fuel injection, and it suggests that combustion did not take place anywhere in the combustion duct. The pitot pressure began to drop when Ta was increased above 1200 K. The intensity of the pressure drop and the extent across the combustion duct increased as Ta increased to 2200 K.[5]

The loss in pitot pressure (ΔP^0) is the sum of two losses in P^0, the first involves the combustion in the flowfield, and the second is from the bow shock wave ahead of the pitot tube. The loss caused by combustion in supersonic flow is several times greater than that in subsonic flow. The large pressure loss caused by supersonic combustion may be compensated by the smaller loss across the bow shock, because the Mach number also decreases by the combustion process. However, in the case of weak and localized autoignition in a freestream tube, the heat release increases the static pressure and expands the cross section of stream tube to relax the pressure. The expansion of the stream tube generates a compression wave. The wave may escape from the exit without impinging the locations monitoring wall pressure, because the weak combustion usually starts near the duct exit.

Thus, the localized combustion in an unconfined freestream is between the Rayleigh process, where heating occurs in a constant-area duct, and the Brayton process, where heating takes place under a constant static pressure. The static pressure does not increase and the Mach number does not decrease as expected from the Rayleigh process. Consequently, the supersonic flow suffers large total pressure loss twice: once in the supersonic combustion process and again in the bow shock upstream of pitot tubes. The large reduction of ΔP^0 found in our experiment is impossible in the combustion in the pitot tube, where the flow is decelerated to subsonic behind the bow shock wave. It is only explainable with supersonic combustion in the combustor duct.

Although the pitot pressure detected the combustion occurring at $Ta > 1200$ K in Fig. 6, the wall pressure distribution along the combustion duct did not indicate the occurrence of combustion until $Ta = 1600$ K. Therefore, the wall pressure is not a suitable indicator of combustion in the supersonic duct, particularly for localized, weak combustion, which requires a long ignition delay time and starts from the combustor exit.

The weak combustion, not to increase wall pressure in combustors, does not contribute to producing the thrust in engines. However, the insensitivity of wall pressure presents an important implication in combustion studies in engines. The development of supersonic combustion along a combustor has often been estimated from the wall pressure distributions. Occasionally, the experimental results have been compared with numerical calculations to calibrate the numerical codes.[16–18] The data presented here indicate that the wall pressure may be less sensitive to small heat release, and that the η_c evaluated by the wall pressure tends to be underestimated.

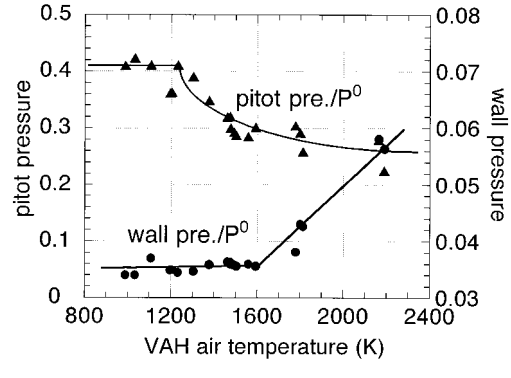

Fig. 6 Detection of combustion by pitot and wall pressures.

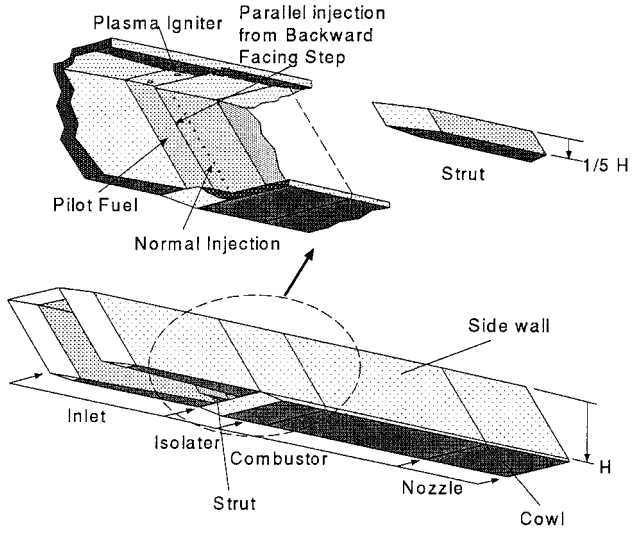

Fig. 7 H_2-fueled scramjet engine tested in National Aerospace Laboratory, Japan.

Application to Scramjet Engine Testing

A scramjet engine that has been tested is shown in Fig. 7 (Ref. 1). The rectangular engine, with a length of 2.1 m, consists of the cowl, the top wall, and two side walls. The entrance and the exit of the engine are 200 wide × 250 mm high (denoted by H). The inlet is a side-wall compression type with 6-deg half-angle. The leading edge is swept back by 45 deg to deflect an airstream for suitable spillage required in starting. The geometrical contraction ratio is 2.86 without struts. Two kinds of struts are prepared: a 50-mm-high ($\frac{1}{5}H$) strut illustrated in Fig. 7, and a 250-mm-high ($\frac{5}{5}H$) strut.

The engine had two 2.5-kW plasma jet (PJ) igniters. Backward-facing steps between the isolator and the combustor are prepared for flame holding. Their heights are 4 mm on the side walls and 2 mm on the top wall. The main H_2 is injected normal from the side walls through 24 holes, or tangentially to the side walls through 24 holes (1.5 mm in diameter) on the steps. The combustion gas expands through the diverging combustion section and the internal nozzle to produce the thrust. The uniformity and the boundary-layer thickness of incoming airflow were calibrated in advance. Wall pressure was measured at about 150 locations, and the heating rate was monitored at about 50 stations on the various parts of the engine.

Gas-sampling and pitot-pressure measurements were made 5 mm downstream of the engine nozzle exit with three, 12-probe rakes, consisting of the probes shown by Fig. 4a. We repeated two or three experiments for each experimental condition to obtain the distributions of gas compositions and pitot pressure at about 70 stations on the exit plane of the engine.

In the engine testing, we need gas composition, pitot pressure, and in-stream, static pressure at the exit of engine to calculate flow properties. For instance, the local mass flux (m) in the engine exit is given using local density (ρ) and velocity (U), as

$$m = \rho U = P_s / RT_s \sqrt{\gamma RT_s} M \tag{9}$$

where R denotes the gas constant of the combustion gas and the static temperature (T_s) is given as a function of M from the isentropic relations, when the total temperature (T_0) is derived from the compositions of sampled gas and the temperature of incoming air (T_a) with the assistance of equilibrium calculations. The Mach number can be estimated from the pitot and the static pressure (P_s) using the Rayleigh pitot formula.

There are three independent measured variables: the T_0, the pitot pressure, and the P_s. Let us examine propagation of errors in these measured variables to the mass flux, assuming the calorically perfect gas for simplicity. Influential coefficients of the variables to the mass flux are defined as partial derivatives:

$$\frac{\Delta m}{m} = \frac{\partial m}{\partial T_0}\frac{\Delta T_0}{T_0} + \frac{\partial m}{\partial P_s}\frac{\Delta P_s}{P_s} + \frac{\partial m}{\partial P_p}\frac{\Delta P_p}{P_p}$$

$$\equiv C_{m,T_0}\frac{\Delta T_0}{T_0} + C_{m,P_s}\frac{\Delta P_s}{P_s} + C_{m,P_p}\frac{\Delta P_p}{P_p} \tag{10}$$

The influential coefficients are expressed using M as the parameter as follows:

$$C_{m,T_0} = -\tfrac{1}{2} \tag{11}$$

$$C_{m,P_s} = 1 - \frac{1}{2}\left\{\frac{M^2 - [(\gamma-1)/2\gamma]}{M^2 - \frac{1}{2}}\right\}\left\{\frac{1+(\gamma-1)M^2}{1+[(\gamma-1)/2]M^2}\right\} \tag{12}$$

$$C_{m,P_p} = \frac{1}{2}\left\{\frac{M^2 - [(\gamma-1)/2\gamma]}{M^2 - \frac{1}{2}}\right\}\left\{\frac{1+(\gamma-1)M^2}{1+[(\gamma-1)/2]M^2}\right\} \tag{13}$$

The influential coefficient of T^0, C_{m,T_0}, is easily understood because the sonic velocity is proportional to $T_0^{1/2}$, and the density is inversely proportional to T_0^{-1} for a given M. The influential coefficient of P_s (C_{m,P_s}) has a maximum value of 0.22 around $M \approx 1.6$, and decreases in $M = 1$ and $M \to \infty$ for $\gamma = 1.4$. On the other hand, the influential coefficient of pitot pressure (C_{m,P_p}), starting from 1 at $M = 1$, has a minimum of 0.78 at $M \approx 1.6$, and finally, approaches 1 as $M \to \infty$. Thus, the mass flux is less sensitive to an error in the static pressure than to that in the pitot pressure.

Voland[19] reports a detail distribution of in-stream static, and wall pressure measured at 13 × 13 stations across the engine exit plane of the NASA Langley Research Center's parametric scramjet engine. The distribution is derived under the no-fuel engine condition, in which the Mach number of internal flow is much higher and deviation between the in-stream and the wall static pressures may become greater than that under fuel-burning conditions. However, the example indicates a maximum deviation of 35% between an in-stream-static pressure in the engine core and the corresponding wall pressure. This fairly uniform distribution and the small influential coefficient of static pressure suggest that the static pressure may be approximated with the local wall pressure measured on the engine exit walls.

A typical mass-flux distribution of air and H_2 measured in weak combustion in the M6 engine testing is illustrated in Fig. 8, when a negligible thrust of 129N was measured with a total fuel $\Phi = 0.30$. In Fig. 8a, the air flux distribution is shown after normalization using the average value; the region greater than 1 is that with a mass flux higher than the average. The contour lines show that the airflow, deflected by the swept-back inlet, is still distorted toward the cowl at the engine exit. More severe distortion was found in the fuel flux

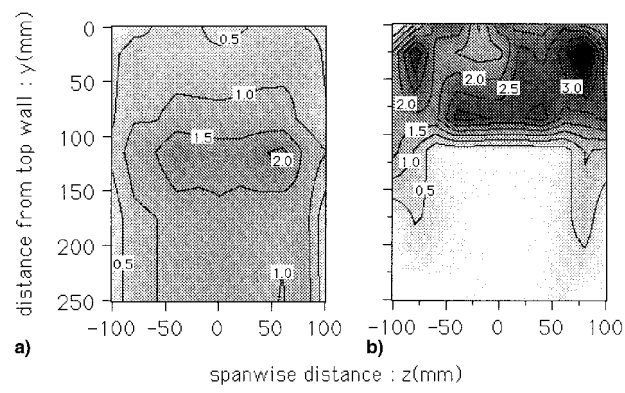

Fig. 8 Mass flux of a) air and b) H_2 in the weak combustion mode.

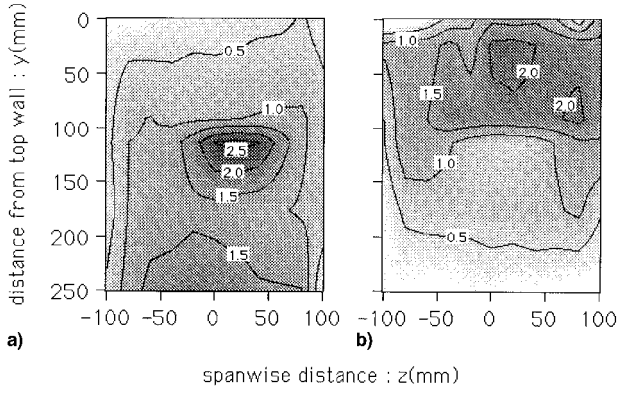

Fig. 9 Mass flux of a) air and b) H_2 in the intense combustion mode.

shown in Fig. 8b. Although the fuel is supplied from injection orifices uniformly distributed on the side walls, H_2 is concentrated near the top wall, especially in the corners between the side walls and the top wall (body side of vehicles). No fuel exists near the cowl. The cause is that the H_2, injected perpendicularly, cannot penetrate the boundary layer developed on the engine walls, and is thus trapped there. Our oil-flow survey using a one-fifth subscaled model indicated a surface flow from the cowl to the top wall downstream from the combustor. The flow is produced by interaction between the boundary-layer flow and the expansion wave in the swept-back, diverging sections. This oil-flow observation supported the finding of H_2 concentrated near the top wall in Fig. 8b.

When the fuel supply rate was increased to $\Phi = 0.42$, the combustion switched from the weak mode to the intense mode, and the engine showed a thrust increment of 1050 N. The engine exhausted a bright flame from the exit. Figures 9a and 9b are the air and H_2 distributions, respectively, in the intense combustion. Although the feature of deflection toward the cowl remains, a dense air region appears in the center of the exit plane. We believe that this is caused by the air deflected by a separation bubble in the engine combustor.

This flow separation improves the mixing of H_2. As a result, the severe distortion of H_2 found in Fig. 8b disappears in the intense combustion in Fig. 9b. Figure 9 indicate that the flowfield is strongly influenced by heat release when combustion takes place in the engine. Thus, gas sampling is informative, not only for measurements of the engine performance, but also for detail investigation of the engine internal flow. The newly designed probes with $0.3d$ orifices were successfully employed in Mach 8 testing.[20]

Conclusions

To assess the reliability of the gas sampling conducted in our scramjet engine testing, we calibrated the quenching ability of reactions in gas-sampling probes. A summary of our theoretical studies and experimental findings follows:

1) Studies using a reduced kinetic model and a full-kinetic code showed that reactions in probes could be extinguished if the cooling Damkohler number was less than about 10.

2) The measurement of the combustion efficiency of H_2 injected into a $M2.5$ supersonic combustor indicated that the probes with a fine tip of 0.3 mm in diameter succeeded in quenching reactions in the probes. However, quenching in the probes with a 0.7-mm tip was found to be insufficient.

3) Pitot pressure was found to be more sensitive than wall pressure to weak combustion in supersonic flow. This implies that the use of wall pressure may lead to underestimation in the combustion efficiency in a supersonic combustor.

4) The validated gas sampling was successfully applied to the scramjet testing under the flight Mach numbers up to 8 to clarify distortions of air and H_2 in the swept-back, side-compression-type engines.

References

[1]Kanda, T., Hiraiwa, T., Mitani, T., Tomioka, S., and Chinzei, N., "Mach 6 Testing of Scramjet Engine Model," *Journal of Propulsion and Power*, Vol. 13, No. 4, 1997, pp. 543–551.

[2]Mitani, T., Hiraiwa, T., Sato, S., Tomioka, S., Kanda, T., and Tani, K., "Comparison of Scramjet Engine Performance in Mach 6 Vitiated and Storage-Heated Air," *Journal of Propulsion and Power*, Vol. 13, No. 5, 1997, pp. 635–642.

[3]Sunami, T., Sakuranaka, N., Tani, K., Hiraiwa, T., and Shimura, T., "Mach 4 Tests of a Scramjet Engine—Effects of Isolator," 13th International Symposium on Air Breathing Engines, ISABE 97-7088, Chattanooga, TN, Sept. 1997.

[4]Billig, F. S., Dugger, G. L., and Waltrup, P. J., "Inlet-Combustor Interface Problems in Scramjet Engines," 1st International Symposium on Air Breathing Engines, Marseille, France, June 1972.

[5]Mitani, T., Chinzei, N., and Masuya, G., "Experiments on Reaction Quenching in Gas Sampling Probes for Scramjet Testing," 27th Symposium (International) on Combustion, Boulder, CO, Aug. 1998.

[6]Anderson, G. Y., and Gooderum, P. B., "Exploratory Tests of Two Strut Fuel Injectors for Supersonic Combustion," NASA TN D-7581, Feb. 1974.

[7]McClinton, C. R., "Interaction Between Step Fuel Injectors on Opposite Walls in a Supersonic Combustor Model," NASA TP 1174, March 1978.

[8]Eggers, J. M., Reagon, P. G., and Gooderum, P. B., "Combustion of Hydrogen in a Two-Dimensional Duct with Step Fuel Injectors," NASA TP 1159, April 1978.

[9]Masuya, G., Kudou, K., Murakami, A., Komuro, T., Tani, K., Kanda, T., Wakamatsu, Y., Chinzei, N., Sayama, M., Ohwaki, K., and Kimura, I., "Some Governing Parameters of Plasma Torch Igniter/Flameholder in a Scramjet Combustor," *Journal of Propulsion and Power*, Vol. 9, No. 2, 1993, pp. 176–181.

[10]Masuya, G., Komuro, T., Murakami, A., Shinozaki, N., Nakamura, A., Murayama, M., and Ohwaki, K., "Ignition and Combustion Performance of Scramjet Combustors with Fuel Injection Struts," *Journal of Propulsion and Power*, Vol. 11, No. 2, 1995, pp. 301–307.

[11]Chinzei, N., Komuro, T., Kudou, K., Murakami, A., Tani, K., Masuya, G., and Wakamatsu, Y., "Effects of Injector Geometry on Scramjet Combustor Performance," *Journal of Propulsion and Power*, Vol. 1, No. 1, 1993, pp. 146–152.

[12]Mitani, T., "Quenching of Reaction in Gas-Sampling Probes to Measure Scramjet Engine Performance," *Proceedings of the 26th Symposium (International) on Combustion*, The Combustion Inst., Pittsburgh, PA, 1996, pp. 2917–2924.

[13]Radhakrishnan, K., and Bittker, D. A., "LSENS, A General Chemical Kinetics and Sensitivity Analysis Code for Homogeneous Gas-Phase Reactions," NASA RP 1329, Feb. 1994.

[14]Reis, V. H., and Fenn, J. B., "Separation of Gas Mixtures in Supersonic Jets," *Journal of Chemical Physics*, Vol. 39, No. 12, 1963, pp. 3240–3250.

[15]Waitz, I. A., Marble, F. E., and Zukoski, E. E., "Investigation of a Contoured Wall Injector for Hypervelocity Mixing Augmentation," *AIAA Journal*, Vol. 31, No. 6, 1993, pp. 1014–1021.

[16]Riggins, D. W., McClinton, C. R., Rogers, R. C., and Bittner, R. D., "Investigation of Scramjet Injection Strategies for High Mach Number Flow," *Journal of Propulsion and Power*, Vol. 11, No. 3, 1995, pp. 409–418.

[17]Northam, G. B., Rogers, R. C., and Diskin, G. S., "CFD Prediction of the Reacting Flowfield Inside a Subscale Scramjet Combustor," AIAA Paper 88-3259, July 1988.

[18]Krishnamurthy, R., Rogers, R. C., and Tiwari, S. N., "Numerical Study of Hypervelocity Flows Through a Scramjet Combustor," *Journal of Propulsion and Power*, Vol. 13, No. 1, 1997, pp. 131–141.

[19]Voland, R. T., "Methods for Determining the Internal Thrust of Scramjet Engine Modules from Experimental Data," AIAA Paper 90-2340, July 1990.

[20]Kanda, T., Wakamatsu, Y., Ono, F., Kudo, K., Murakami, A., and Izumikawa, M., "Mach 8 Testing of a Scramjet Engine Model," AIAA Paper 99-0617, Jan. 1999.